Investigations on the effect of different ultrasonic amplitudes and positions in the vibration distribution on the microstructure of laser beam welded stainless steel

Nothdurft, Sarah, Ohrdes, Hendrik, Twiefel, Jens, Wallaschek, Jörg, Hermsdorf, Jörg, et al.

Sarah Nothdurft, Hendrik Ohrdes, Jens Twiefel, Jörg Wallaschek, Jörg Hermsdorf, Ludger Overmeyer, Stefan Kaierle, "Investigations on the effect of different ultrasonic amplitudes and positions in the vibration distribution on the microstructure of laser beam welded stainless steel," Proc. SPIE 11273, High-Power Laser Materials Processing: Applications, Diagnostics, and Systems IX, 112730J (2 March 2020); doi: 10.1117/12.2566035

SPIE.

Event: SPIE LASE, 2020, San Francisco, California, United States

Investigations on the effect of different ultrasonic amplitudes and positions in the vibration distribution on the microstructure of laser beam welded stainless steel

Sarah Nothdurft*[a], Hendrik Ohrdes[b], Jens Twiefel[b], Jörg Wallaschek[b], Jörg Hermsdorf[a], Ludger Overmeyer[a], Stefan Kaierle[a]
[a]Laser Zentrum Hannover e.V., Hollerithallee 8, Hannover 30419, Germany
[b]Institut für Dynamik und Schwingungen, Appelstraße 11, Hannover 30167, Germany

ABSTRACT

Laser beam welding is a necessary and helpful tool in modern production technology. It provides low and located heat input, narrow weld widths, high welding speeds and weld depths. Nevertheless, in the weld metal and the surrounding area the microstructure and the mechanical characteristics can be changed afterwards. A decrease of strength and fatigue life is a possible result. To realize a manipulation or control of the weld metal's microstructure during the welding process is a great challenge. Improving the strength as well as the homogeneity of mechanical properties and chemical composition are the aims of this approach. With indirect introduced ultrasonic amplitudes, the weld pool dynamics and the solidification are affected.

The investigation focusses on the effects in the microstructure of high power (8 kW) laser beam welded stainless steel (AISI 304) with weld depths up to 15 mm. For two different amplitudes (3 and 6 µm) and three different positions of the weld pool in the vibration distribution (antinode, centered and node position) the weld metal is evaluated with metallographic cross sections. The types and the amount of microstructures are analyzed. The solidification of the weld metal is influenced by the vibration. Thus, the orientation, size and growth of the grains as well as the growth direction are changed. Furthermore, the weld characteristics (weld depth, weld width, weld area) are compared to the previously considered aspects.

Keywords: laser beam welding, stainless steel, AISI 304, ultrasound, microstructure

1 INTRODUCTION

Shaping the weld's microstructure in different ways according to their intended purposes is of high interest. Mechanical properties, corrosion resistance, ductility and application temperature can be influenced. So the grain size, segregations, precipitations or intermetallic phases show huge effects on the before mentioned characteristics. As diverse as the materials used nowadays and their requirements are, so it is important to look across disciplines and borders on methods to influence the formation of the microstructure and geometry of the weld metal.

For liquid metals besides welding as well for laser additive manufacturing of AISI 630 stainless steel ultrasonic vibrations were used for a reduction of balling effect. Furthermore, the geometrical dimensions in molten pool and dilution zone were increased with the result of improved bonding strength [1]. The method was able to reduce or eliminate the defects and achieved grain refinement and therefore an improvement of mechanical properties. For ultrasonic assisted laser surface processing of AISI 316 the vibration delays the interaction between laser and the material according to [2], increasing with higher ultrasonic amplitude [2]. Furthermore, the melt is expulsed and the solidified remaining surface films show a transition from columnar to equiaxed dendritic grain structure. The width and the depth of the molten area are higher for lower amplitudes than for higher amplitudes.

For ultrasonic vibration assisted pulsed laser welding of Hastelloy C-276 and AISI 304 the weld shape changed and the weld depth increases as well as the mixing. The texture in the weld metal was changed with the chance of improving ductility [3]. Cavitation was visible for high ultrasonic amplitudes.

*s.nothdurft@lzh.de; phone 0049 511 2788 365; fax 0049 511 2788 100; lzh.de

High-Power Laser Materials Processing: Applications, Diagnostics, and Systems IX, edited by Stefan Kaierle, Stefan W. Heinemann, Proc. of SPIE Vol. 11273, 112730J · © 2020 SPIE
CCC code: 0277-786X/20/$21 · doi: 10.1117/12.2566035

In previous investigation was shown that ultrasonic amplitude has an influence on the dynamics in the weld pool and as a result on the mixing in the weld metal [4] and the position in the vibration distribution influence the geometry and the microstructure of the weld metal for a widely used aluminum alloy (AA6082) as well [5]. The solidification of the weld metal is influenced by the vibration, the orientation, the direction and size of the grains and their growth is changed. Another widely used class of material are steels. In the group of stainless steels nearly 33 % are accounted by grade AISI 304.

Iron (as main alloying element in steel) has in comparison to aluminum (as main alloying element of aluminum alloys) mainly different characteristics in solid and liquid state. Viscosity of iron melt is more than five times higher than the viscosity of aluminum melt [6], also the surface tension of the iron melt is twice the surface tension of aluminum melt [6] and density of iron is three times the density of aluminum. Which differences and similarities in the behavior of melt and the formation of the microstructure in the weld metal for ultrasonic excitation result from these characteristics is the topic of this publication.

The following effects of the microstructure on the properties of stainless steels are already known. Corrosion resistance increases with decreasing grain size [7]. Furthermore, the angel of the grains respectively the solidification which causes the direction influences the resistance against cracks. This advantageous direction is possible for laser beam welding with CO_2 laser beam source of sheets with more than 1.2 mm sheet thickness [8]. The formation of microstructure and the ferrite to austenite ratio is dependent on the heat input. Fast solidification, which is characteristic for laser beam welding processes with high intensities, high laser beam power and high welding speeds, leads to incomplete $\delta \rightarrow \gamma$ transformation and metastable δ-ferrite [9]. In comparison with TIG and laser TIG hybrid welding, the dendrites size for laser beam welded joints is the smallest.

2 EXPERIMENTAL SETUP

2.1 Ultrasound system

The ultrasonic system was designed to generate a vibration with approximately 20 kHz in the workpiece, which is part of the vibration system. To prevent a clattering of the workpiece due to dynamic forces, a hydraulic clamping system was used. The current amplitude and phase of the transducer were controlled by the DPC500/100k [10, 11], which was developed at the Institute of Dynamics and Vibration Research. The position in the vibration distribution of the welding area was adapted by moving the welding head to the desired position. With a fiberoptic laservibrometer the velocity was measured to identify the vibration maximum (antinode) and the vibration minimum (node). Figure 2 shows a calculation of the vibration distribution along the workpiece. By means of the measured relation between driving current and the amplitude in the antinode position, calculation of amplitude (cf. explanations for Figure 2) and stress at every position is possible.

2.2 Laser beam welding system

The laser beam source used for the welding tests was a diode-pumped, solid state disk laser (Trumpf TruDisk 16002), with a maximum output power of 16 kW and a wavelength of 1,030 nm. The high power welding head (Precitec YW52) with a collimation length f_C of 150 mm and a focal length f_F of 300 mm was guided by a robot system and created by using a fiber with a diameter of 200 µm a focal spot diameter of 400 µm. The welding speed was initiated by the motor of the ultrasound system. The experimental setup is shown in Figure 1.

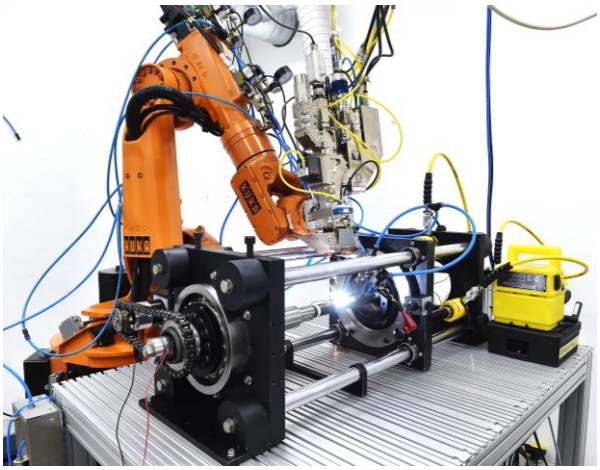

Figure 1. Experimental setup for the ultrasound assisted laser beam welding (source: LZH)

3 EXPERIMENTAL PROCEDURE

The tests were performed on round bars made of AISI 304 (1.4301/X5CrNi8-10 [mass fraction as follows $C \leq 0.07$ %, $Si \leq 1.00$ %, $Mn \leq 2.00$ %, $P \leq 0.045$ %, $S \leq 0.015$ %, $Cr \leq 17.50\text{-}19.50$ %, $Ni \leq 8.00\text{-}10.50$ %, $N \leq 0.11$ %]) with a diameter of 30 mm and a length of 170 mm. The samples were clamped with 200 bar hydrostatic pressure. Three different positions in the waveform of the vibration distribution (node, centered and antinode position) and two different ultrasound amplitudes (3 µm and 6 µm) were examined. The amplitude referred to is the amplitude in the antinode. Because of the sinusoidal shape (grey dotted line) of the vibration distribution (cf. Figure 2), the vibration amplitude is half of the referred amplitude on the centered position and there is no amplitude at the node position (red part of the graph). The stress value shows an exactly inverse behavior.

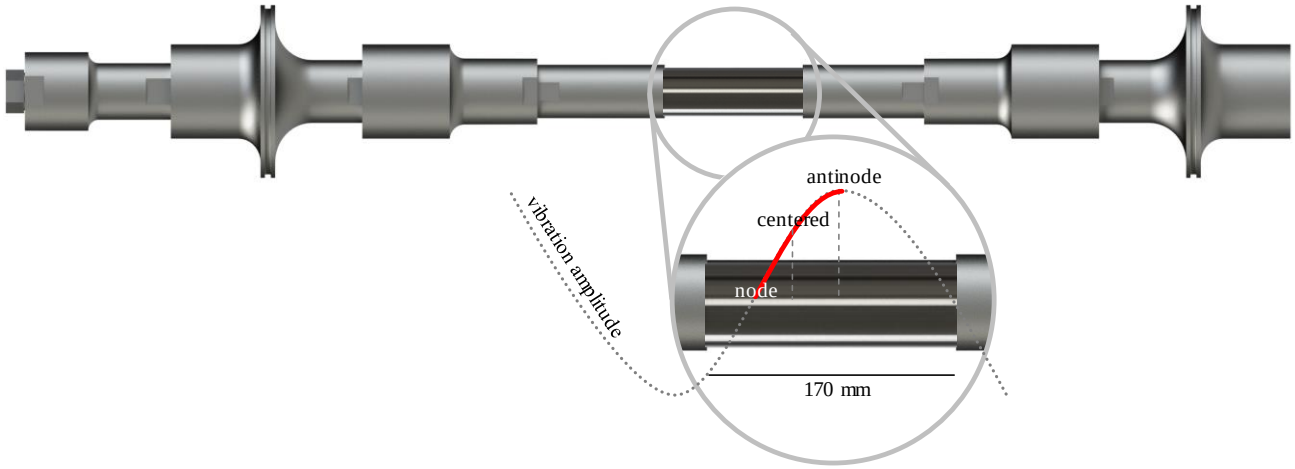

Figure 2. Graphical representation of the vibration system with a magnification of the sample with the welding positions

The welding parameters used were a laser beam power P_L of 8.0 kW and a welding speed v_F of 0.95 m/min. The focal z-position was 4 mm below the surface. The parameters of the samples 0 and A to G are listed in Table 1. Each parameter configuration was repeated two times for statistical confidence. In addition, samples with the parameter 0 were made for a comparison with the weld characteristics without ultrasonic excitation as a reference.
Metallographic cross sections were prepared for each sample. Thus, four cross sections result for analyses for each parameter. Weld width, weld depth, weld metal area, microstructure and micro hardness were identified and evaluated, these results are introduced and discussed in the following chapter.

Table 1. Parameter configurations

value unit	position	amplitude µm	laser beam power kW	welding speed m/min
0	-	0	8	0.95
A	node	3	8	0.95
B	node	6	8	0.95
C	centered	3	8	0.95
D	centered	6	8	0.95
E	antinode	3	8	0.95
F	antinode	6	8	0.95

4 RESULTS AND DISCUSSION

4.1 Visual inspection

The visual inspection is the first step for characterizing welds. In this case, big differences and the influence of the ultrasonic amplitude on the weld reinforcement are obvious. Figure 3 shows some exemplary photographs of the top view for each parameter configuration. With increasing amplitude, the weld becomes more irregular, melt is ejected from the weld pool. For antinode and centered position big spatters come down on the side which is stimulated from the sonotrode. There is sagging in the middle of the weld. Except for the spatter formation the impact of the vibration is similar to the AA6082 welds.

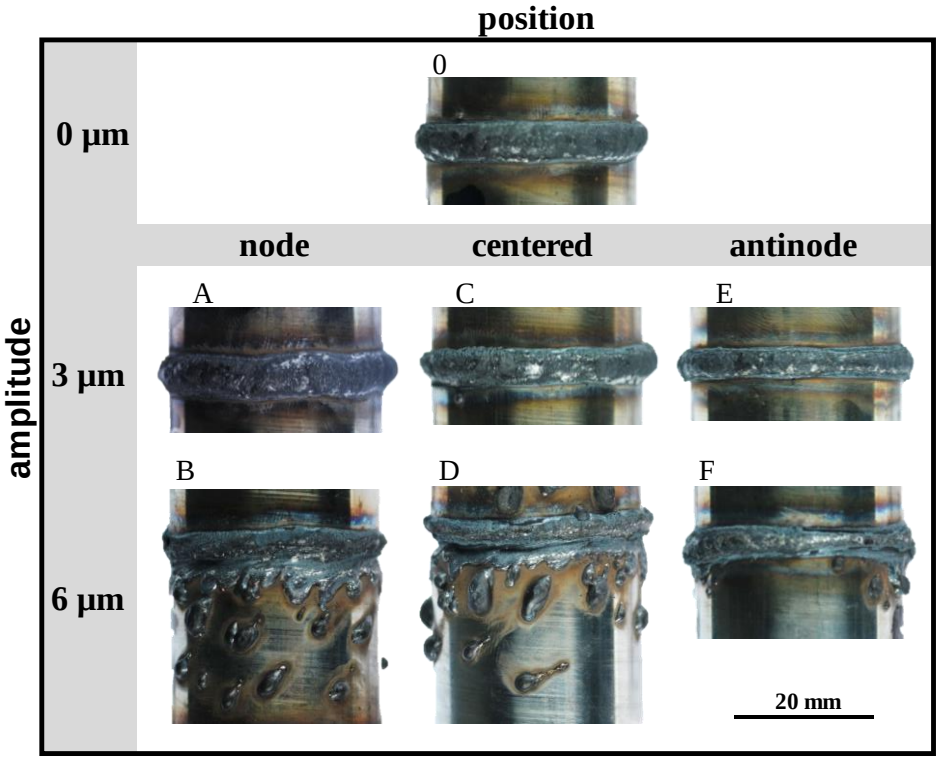

Figure 3. Photographs of the top view: exemplary for each parameter configuration

4.2 Weld metal

To verify the findings from the visual inspection, which is just a superficial evaluation, metallographic cross sections of the weld metal sections were made. As expected, micrographs of metallographic cross sections show significant differ-

ences for the parameters. Figure 4 is an overview of the different welds, the red boxes mark the areas where the enlargements in Figure 9 originate. The geometric characteristics were measured and analyzed. Table 2 presents the results. Measured values are the weld area, the weld depth, the weld width and the angel of the weld compared to the vertical line. The standard deviation (SD) is included.

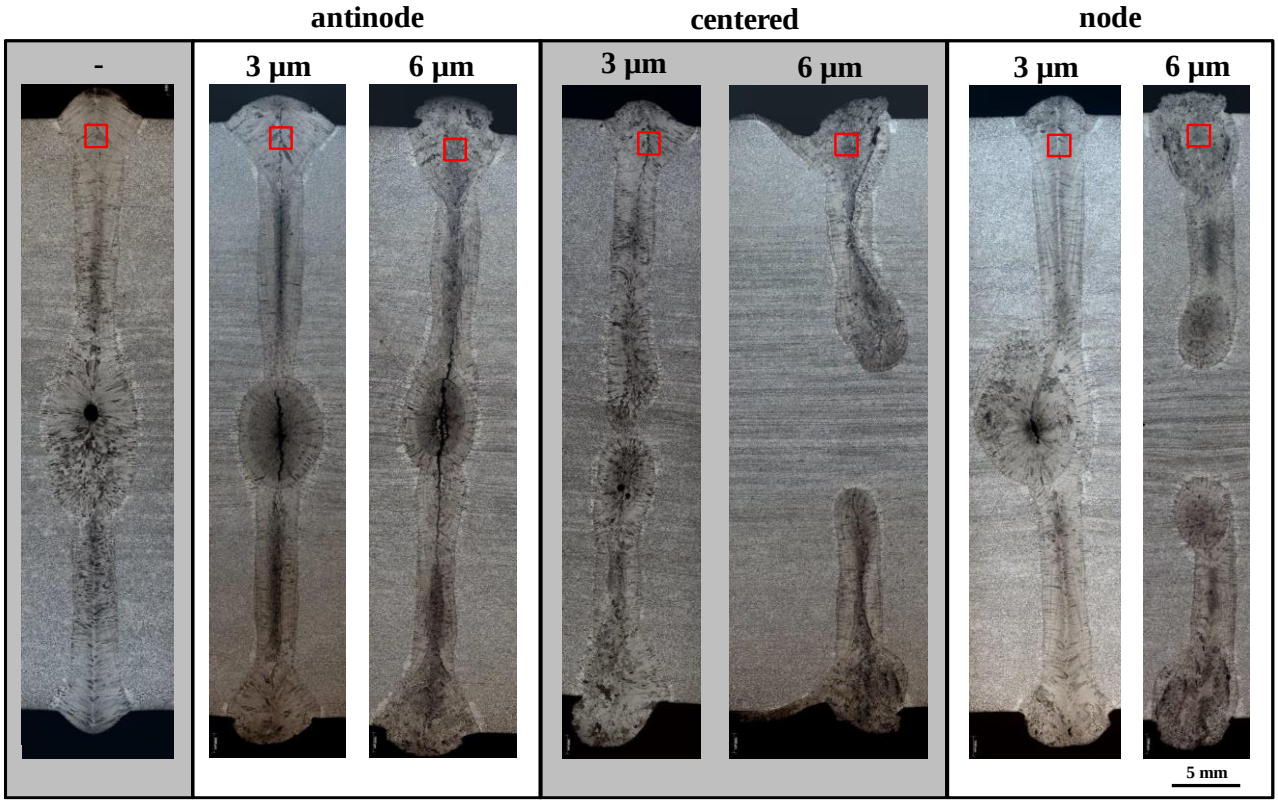

Figure 4. Comparison of exemplary micrographs of metallographic cross sections for the different positions and amplitudes (red boxes show position of enlargements in Figure 9)

Table 2. Geometric characteristics

value	position	amplitude	area	SD	weld depth	SD	weld width	SD	angel	SD
unit		µm	mm^2		mm		mm		°	
0	-	0	40.26	6.8	19.5	1.0	4.20	0.8	1.14	0.5
A	antinode	3	43.31	1.7	17.1	1.9	4.50	0.3	3.56	1.8
B	antinode	6	39.54	3.9	14.0	1.6	4.75	0.8	3.34	0.8
C	centered	3	42.67	4.2	15.2	1.3	4.80	0.2	1.50	4.1
D	centered	6	37.86	3.7	11.9	0.7	6.90	1.4	6.20	1.5
E	node	3	43.37	4.2	16.8	1.7	5.11	0.4	1.69	0.6
F	node	6	46.35	7.3	15.4	1.4	5.23	0.5	0.95	1.6

It can be seen, that the weld depth decreases with increasing amplitude. For the node position is even with an amplitude of 6 µm (contrary to centered and antinode position, where the weld depth decreases significantly) the weld depth higher than 15 mm (cf. Figure 5, right), which is half of the diameter of the round bars. This causes an overlay of the weld in the root area. For the node position, the stress is highest and the amplitude is zero, so the keyhole and therefore the keyhole depth remain stable at all vibration amplitudes investigated. The angel of the weld compared to the vertical line shows strong differences, but varies too much for each parameter for a sufficient evaluation.

In the node position (Figure 5, left) there is a small influence on the weld metal area for the different amplitudes. The weld metal area increases slightly for increasing amplitude. For centered (Figure 6, left) and antinode position (Figure 7, left) there is no or just a little influence. The weld depth is decreasing for all positions (Figure 5, right, Figure 6, right, Figure 7, right), but the smallest effect is there for node position. The weld width is increased most for centered position as a result the weld width to weld depth ratio increases alike the most. The effects on weld depth, weld width and weld metal area are similar to the findings from the investigations with AA6082 aluminum alloy.

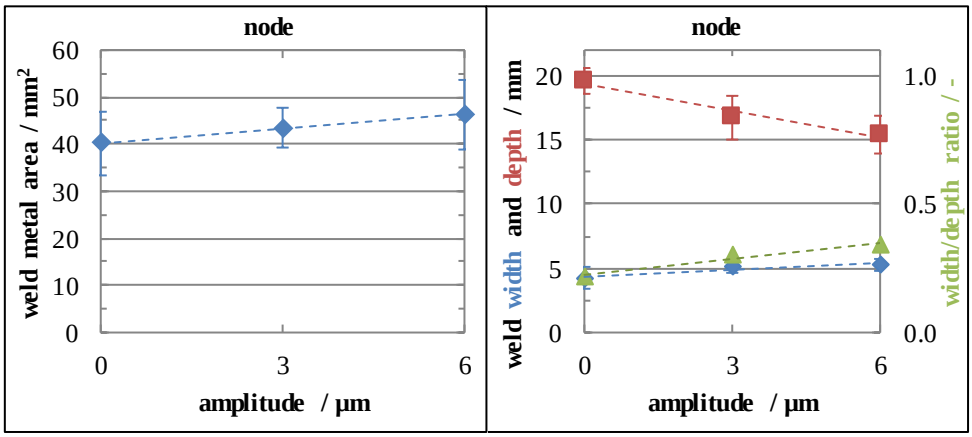

Figure 5. Correlation between amplitude and weld metal area (left), weld width, weld depth and width/depth ratio (right) for node position

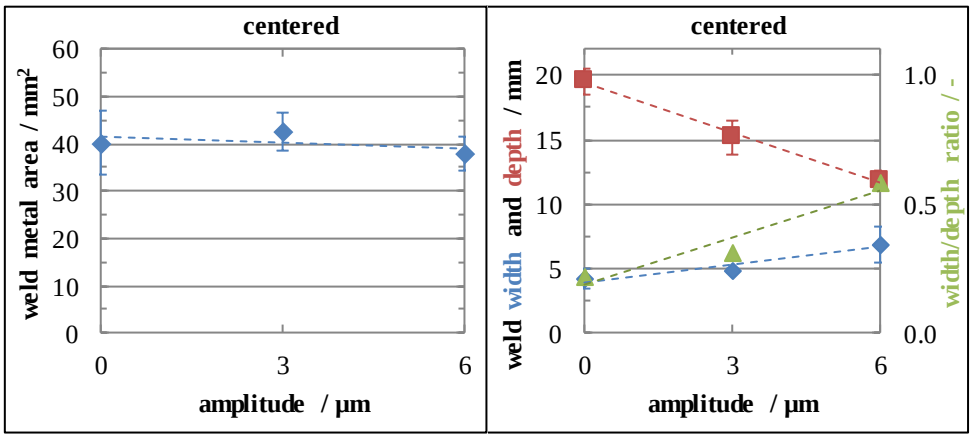

Figure 6. Correlation between amplitude and weld metal area (left), weld width, weld depth and width/depth ratio (right) for centered position

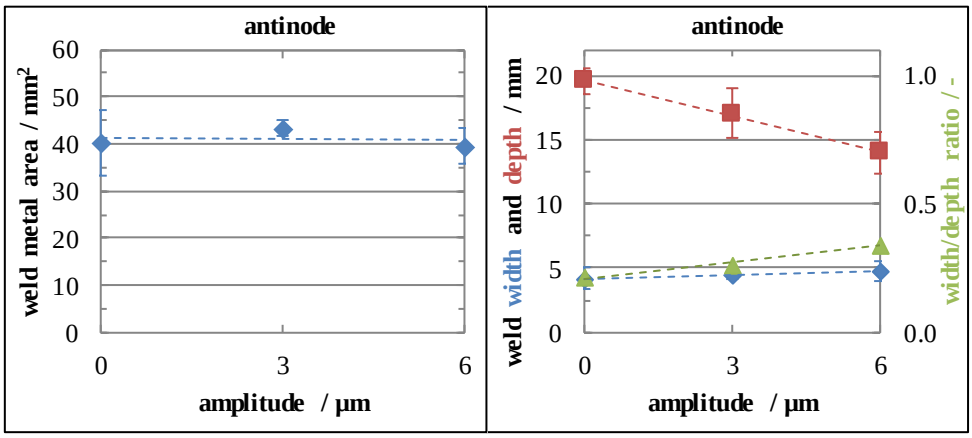

Figure 7. Correlation between amplitude and weld metal area (left), weld width, weld depth and width/depth ratio (right) for antinode position

4.3 Solidification

As visible in Figure 9 (and already shown in Figure 4) for some samples cracks occur. Over the whole number of samples there are cracks in most of the welds with amplitudes in the node and centered position. For samples without amplitude or in the antinode position, no cracks appear on the samples taken. The case of loading in the different positions is a possible reason. For the antinode position there is high amplitude and no stress in the joining zone. The real amplitude for centered position is half of the amplitude of the reference (antinode position) and half of the stress referred to the node potion (cf. Figure 2 and the explanation). Node position has no amplitude but highest stress. The stress seems to strain the liquid and solidifying metals that much that cracks appear in the middle of the weld metal. A scanning electron microscope (SEM) micrograph shows a fracture surface, as expected it is a hot crack, evident from the visible free dendrites ends.

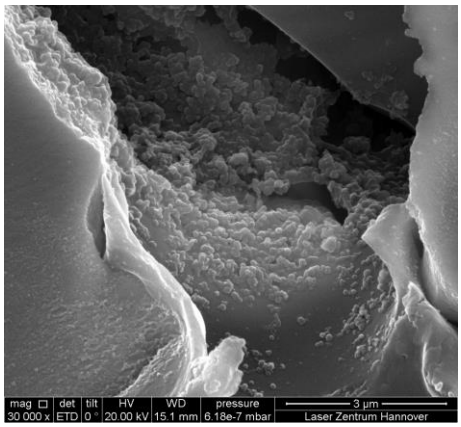

Figure 8. SEM micrograph of a fracture surface for a sample with an amplitude of 3 µm in node position

Another aspect is the evolved microstructure that shows best in enlargements with high resolution in the upper middle of the weld metal (Figure 9, the areas where the enlargements originate are marked with red boxes in Figure 4). The structure and orientation of the microstructure exhibit strong differences. For the samples with no amplitude and 3 µm amplitude dendritic structure is visible, which form different areas and directions. The angles of the dendrites were measured over the section shown. Table 3 and Figure 10 present the results. For an amplitude of 6 µm no dendrites are visible, so they are not considered here. The value of the centered position matches the value of the sample without amplitude, also the value of the antinode position is near this value. The node position shows a much smaller angel and shorter dendrites which may again be caused by the highest stress value in this position. These points are evidences for the influence of the ultrasonic vibration on the solidification in the weld metal.

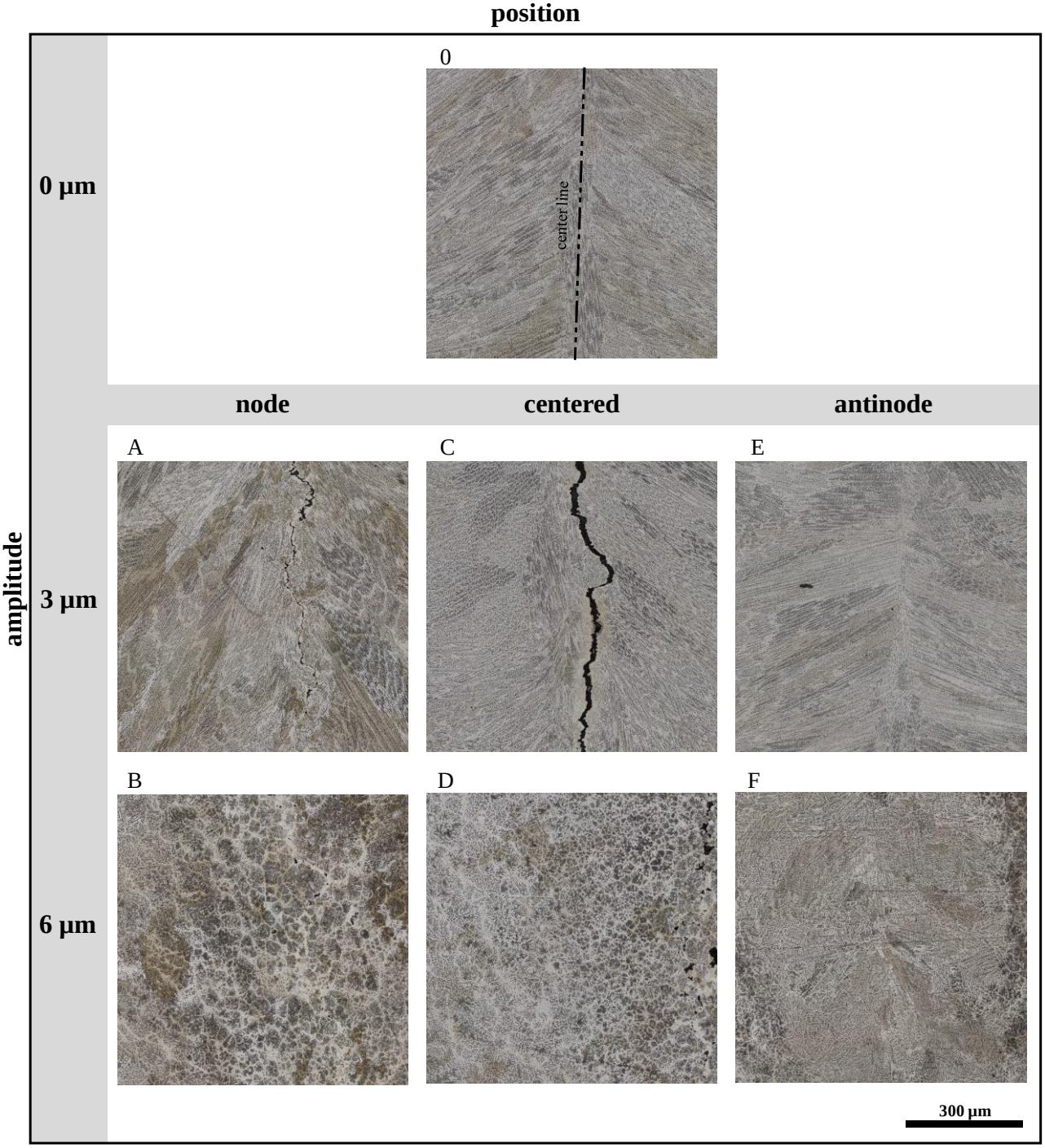

Figure 9. Enlargements from the center of the weld taken from micrographs of cross sections: exemplary for each parameter configuration (cf. Figure 4 for position of the enlargements)

Table 3. Solidifying characteristics in the weld metal

value unit	position	amplitude µm	angel of dendrites °	SD
0	-	0	73.87	2.66
A	node	3	51.20	7.65
B	node	6	-	-
C	centered	3	76.86	10.14
D	centered	6	-	-
E	antinode	3	69.86	7.57
F	antinode	6	-	-

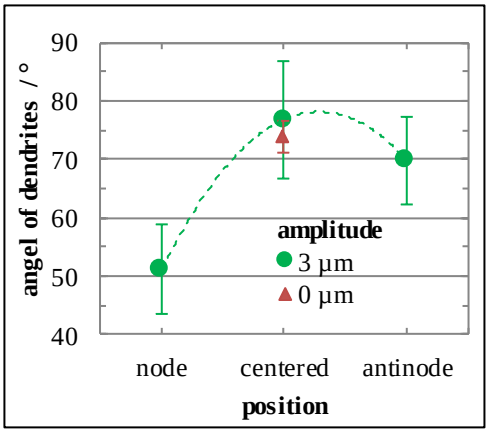

Figure 10. Comparison of exemplary micrographs of metallographic cross sections for the different positions and amplitudes

The 6 µm samples show no center line and no dendrites, respectively dendrites form only in the edge zone near the fusion line because the solidification begins in this place and has high solidification speed. The effect on the melt arising from the vibration is not fast or strong enough for an influence in this area. Austenite precipitation starts on ferrite grain boundaries, due to the interruption of the solidification no dendrites form and δ-ferrite remains plate-shaped in the austenite matrix. Figure 11 gives a close look on the dominant microstructure for the unaffected weld metal and the weld metal in node position with an amplitude of 6 µm.

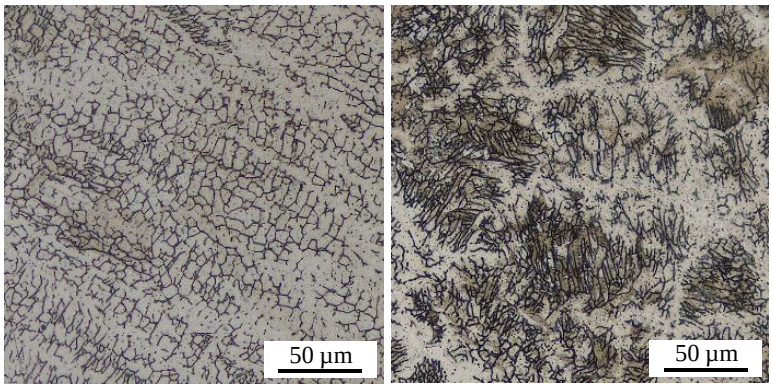

Figure 11. Enlargement of the weld metal of the sample without vibration (left) and with an amplitude of 6 µm in node position (right)

As the weld metal area is nearly the same for all samples, due to this the heat input during the welding process had to be similar. An explanation is that the dendrites are interrupted by the vibration and break and so the solidification changes its direction. This is more obvious for the higher amplitudes, but also for 3 µm as pointed out with the measurement of the angel of dendrites. Furthermore, hardness tests were performed. As a result of this test no differences in the average

hardness, the minimal and maximal hardness value in the weld metal or the shape of the graph connecting the points in the diagrams are apparent.

5 CONCLUSION

In this paper the effects of amplitude and position in the vibration distribution in the joining zone for laser beam welding of AISI 304 is presented and discussed. In summary the following conclusions were drawn:
The amplitude is the biggest influence, an amplitude of 3 µm and the sample without amplitude show for the welding and ultrasonic parameters chosen slight differences. An amplitude of 6 µm causes strongly changed microstructure (caused by preventing the formation of dendritic structures) and weld depth (caused by producing a collapse of the keyhole).
However, the position of the amplitude in the vibration distribution is also a relevant parameter. It influences the angel of the dendrites, as long as they form (up to 3 µm for the welding and ultrasonic parameters chosen). In addition, the formation of cracks is affected by the position due to the stress loading especially in the center line. So cracks appear for high stresses (node position).
As shown, it is possible to influence the grain size and the microstructure. Due to the huge impact of these parameters, an improvement and customization according to the requirements is feasible. This means an adjustability of as example strength of a joint, homogeneity in the weld metal as well as in the mechanical properties, which furthermore can be improved. Therefore, further investigations and tests are necessary.

ACKNOWLEDGEMENTS

The results presented in this publication were obtained from the Collaborative Research Centre 1153 “Process chain to produce hybrid high performance components with Tailored Forming” in subproject A3. The authors would like to thank the German Research Foundation (DFG) for the financial and organizational support of this project.

REFERENCES

[1] Cong, W., and Ning F., “A fundamental investigation on ultrasonic vibration-assisted laser engineered net shaping of stainless steel”, International Journal of Machine Tools and Manufacture 121, 61-69 (2017).
[2] Alavi, S. H., Harimkar, S. P., “Melt expulsion during ultrasonic vibration-assisted laser surface processing of austenitic stainless steel”, Ultrasonics 59, 21–30 (2015).
[3] Zhou, S., Ma, G., Wu, D., Chaa, D., Leib, M., “Ultrasonic vibration assisted laser welding of nickel-based alloy and austenite stainless steel”, Journal of Manufacturing Processes 31, 759–767, (2018).
[4] Nothdurft, S., Seffer, O., Lahdo, R.; Hermsdorf, J., Kaierle, S., “Laser beam joining of dissimilar joints of steel and aluminium alloys”, Welding and Cutting 17 (5), 392-398 (2018).
[5] Nothdurft, S., Ohrdes, H., Twiefel, J., Wallascheck, J., Mildebrath, M.; Maier, H. J., Hassel, T., Overmeyer, L. and Kaierle, S., “Influence of ultrasonic amplitude and position in the vibration distribution on the microstructure of a laser welded aluminum alloy,” Journal of Laser Applications 30 (3), (2019).
[6] Valencia, J. J., Quested, P. N., [Thermophysical Properties ASM Handbook Volume 15: Casting], 468-481 (2008).
[7] Di Schino, A., Kenny, J. M., “Effects of the grain size on the corrosion behavior of refined AISI 304 austenitic stainless steels”, Journal of materials science letters 21 (20), 1631–1634 (2002).
[8] Nath, A., Sridhar, R., Ganesh, P., Kaul, R., “Laser power coupling efficiency in conduction and keyhole welding of austenitic stainless steel”, Sadhana 27 (3), 383–392 (2002).
[9] Yan, J., Gao, M., Zeng, X., “Study on microstructure and mechanical properties of 304 stainless steel joints by TIG, laser and laser-TIG hybrid welding”, Optics and Lasers in Engineering 48 (4), 512–517 (2010).
[10] Twiefel, J., Klubal, M., Paiz, M., Mojrzisch, S. & Krüger, H., “Digital signal processing for an adaptive phase-locked loop controller”, Proc. of SPIE 6926, (2008).
[11] Ille, I. & Twiefel, J, “Model-Based Feedback Control of an Ultrasonic Transducer for Ultrasonic Assisted Turning Using a Novel Digital Controller”, Physics Procedia 70, 63-67 (2015).